Does the Predictability of ENSO Depend on the Seasonal Cycle?

MORITZ FLÜGEL AND PING CHANG

Department of Oceanography, Texas A&M University, College Station, Texas

(Manuscript received 17 April 1997, in final form 12 December 1997)

ABSTRACT

An intermediate coupled ocean–atmosphere model that permits dynamical interactions between the seasonal cycle and interannual oscillations is used to conduct large ensembles of ENSO prediction experiments. By varying seasonal backgrounds, the impact of the annual cycle on the model's forecast skills is explored. The results show that the sensitivity of the skills to changes in the seasonal cycle is weak, although correlation skills drop and rms errors increase systematically by a small amount as the amplitude of the seasonal cycle is enhanced. This suggests that the nature of the model's prediction skills is largely determined by the seasonal information hidden in the initial conditions and the actual varying seasonal background is of secondary importance.

As in other anomaly coupled models, the spring predictability barrier is a predominant feature of this model's prediction skills. This seasonal dependence of the forecast skills exhibits a decadal modulation with strong barriers in the 1960s and 1970s and weak ones in the 1950s and 1980s. The best skills of the model occur in the 1950s and 1980s and the worst in the 1970s. The decadal modulation of the skills is more likely to come from decadal shifts in the mean state of the tropical Pacific than from nonlinear interactions between the seasonal cycle and interannual oscillations.

1. Introduction

The El Niño–Southern Oscillation (ENSO) phenomenon is the strongest climate signal on interannual timescales. Although ENSO arises from a coupled ocean–atmosphere interaction in the Tropics, it has far-reaching impacts on global weather patterns. The predictability of this phenomenon has thus been a central concern for climate research in the past decade. The basis for ENSO forecast is provided by the fact that the positive feedback between the tropical ocean and atmosphere determines, to a certain degree, the future low-frequency time evolution of the coupled system.

Skillful ENSO forecasts have been demonstrated with a large variety of models ranging from purely statistical models (Barnett 1984; Barnett et al. 1988; Graham et al. 1987; Xu and von Storch 1990; Penland and Magorian 1993) to intermediate (Cane et al. 1986; Zebiak and Cane 1987; Balmaseda et al. 1995), hybrid coupled models (Barnett et al. 1993; Latif and Flügel 1991), and fully coupled ocean–atmosphere general circulation models (GCMs) (Latif et al. 1993; Leetmaa and Ji 1989; Rosati et al. 1995). Although these models have all demonstrated certain capability of predicting the ENSO-related sea surface temperature (SST) anomalies several seasons in advance, predictive skills vary considerably from model to model. With the exception of the coupled GCMs, the seasonal cycles of the SST and wind in these models are either prescribed or absent, thereby only allowing for interactions among the anomaly patterns. The skillful forecasts achieved by these anomaly models, especially the Lamont model (Zebiak and Cane 1987; Chen et al. 1995), argue that, to a certain degree, abandoning an ''active'' seasonal cycle in modeling ENSO may be justified. However, there are at least three reasons for a closer examination of the effects of the annual cycle on ENSO predictions.

First, it is well known from the observations that ENSO tends to be strongly phase locked to the annual cycle, in a sense that nearly every extreme warm phase occurs in winter (e.g., Rasmusson and Carpenter 1982). This suggests that there is indeed an interrelationship between the seasonal cycle and interannual variability. An improved understanding of this interrelationship may assist in more accurate prediction of ENSO.

Second, it has been hypothesized in several recent studies that nonlinear interactions between the interannual variability and the annual cycle might be responsible for the irregular oscillatory behavior of ENSO (Jin et al. 1994; Tziperman et al. 1994; Chang et al. 1995). This raises the possibility that ENSO predictability may be affected by the nonlinear dynamics involved in feedbacks between the seasonal cycle and interannual oscillations.

Third, the seasonal cycle of SST in the eastern Pacific

Corresponding author address: Dr. Moritz Flügel, Department of Oceanography, Texas A&M University, College Station, TX 77843-3146.
E-mail: fluegel@mako.tamu.edu

Ocean is not a simple response to the change in solar radiation; it is influenced by complex dynamic and thermodynamic feedbacks between the tropical atmosphere and equatorial ocean (Mitchell and Wallace 1992; Chang and Philander 1994; Xie and Philander 1994; Philander et al. 1996). Because of these feedbacks, the amplitude of the seasonal cycle is modulated by the interannual variability (Gu and Philander 1995). Many coupled GCMs that attempt to include these feedbacks have considerable difficulty reproducing the observed seasonal cycle with respect to phase, amplitude, and spatial structure (Mechoso et al. 1995). It is often assumed that these models would encounter severe problems forecasting ENSO because of the unrealistic seasonal background.

For all these reasons, it is of general interest to consider how a variation in either the amplitude or phase of the annual cycle might influence certain properties of the coupled ocean–atmosphere system such as the oscillatory behavior or predictive skill. The impact of the seasonal cycle on the oscillatory behavior of ENSO has been addressed by several previous studies (e.g., Chang et al. 1996; Jin et al. 1996; Tziperman et al. 1994). The present study focuses on the issue concerning the effect of the seasonal cycle on ENSO predictability. The problem can be conveniently studied with an intermediate model recently developed by Chang et al. (1996), because it allows for explicit phase shifts and amplitude alterations in the surface heat flux forcing that maintains the seasonal cycle.

A detailed description of the model is given in section 2, along with a demonstration of the model's ability to simulate simultaneously the annual cycle and interannual variability. The skill of model ENSO forecast is investigated in section 3. In section 4 an attempt is made to shed some light on the role of the annual cycle in ENSO predictions by carrying out several sensitivity experiments in which the phase and amplitude of the seasonal forcing are varied. Finally, section 5 gives a summary and a discussion of the results.

2. Intermediate coupled model

The model used in this study consists of an empirical atmospheric feedback and a reduced gravity ocean. The atmospheric component has no internal variability, and thus the entire memory of the coupled system lies in the ocean. In this simplified framework the near-surface wind stress is assumed to be largely determined by the SST in such a manner that winds adjust instantaneously in the atmospheric boundary layer to changes in the SST. This assumption holds well for the low-frequency variability in the Tropics.

The model was constructed from 30 years (1960–89) of observed SST and surface wind stress data in the tropical Pacific derived from the Comprehensive Oceans–Atmosphere Data Set (COADS) (Woodruff et al. 1987) with additional quality control and processing by A. M. da Silva et al. (1995, personal communication). The approach in this study, which was first used by Chang et al. (1996), differs from the empirical feedback models in earlier investigations (Latif and Flügel 1991; Barnett et al. 1993; Balmaseda et al. 1995) in that the coupling is based on the leading (eight) empirical orthogonal functions (EOFs) of observed total SST and surface wind stress perturbation in the tropical Pacific, instead of the interannual fields. Thus, prior to the EOF analysis, only the annual means, rather than the annual cycles, of the wind and SST fields were removed. The first two dominant modes are largely associated with the annual cycle, while the remaining six higher EOFs contain information about the interannual variability. The chosen number of accounted EOFs is based on the experience in Barnett et al. (1993): Too many EOFs favor small-scale high-frequency processes, while too few EOFs may result in loss of essential information. Correspondingly, the feedback matrix was calculated by linear regression between the first eight principal components of the temperature and wind stress EOFs. The empirical wind stress EOFs can then be derived by applying this coupling matrix to the EOF time series of a given SST field.

By definition the atmospheric feedback only accounts for the low-frequency variability, because the higher EOFs were neglected. Due to the absence of the high-frequency component, it is necessary to introduce a scaling factor, δ, into the interannual component of the the wind field. In this study we use this parameter δ to vary the strength of ocean–atmosphere feedbacks. This coupling parameter controls the embedded nonlinearity of the coupled system.

The oceanic component is a derivate of the Lamont model (Zebiak and Cane 1987), which has successfully performed a number of ENSO forecasts and has been widely used in various ENSO modeling studies. The model has an interface between two immiscible layers of fluid, each of constant density, which simulates the sharp and shallow tropical thermocline separating the warmer mixed layer at the surface from the colder deeper water. The motion in the upper layer obeys the conservation laws for mass and momentum, while the lower layer is assumed to be infinitely deep and motionless. Embedded within this 1½-layer reduced gravity ocean is a constant depth, linear Ekman layer to capture the intensity of wind-driven surface currents and the associated vertical motion. The surface temperature is calculated using an entrainment (upwelling) velocity computed from the divergence of the surface currents. This simple model includes both the surface and the subsurface dynamics in a crude way. The model was originally developed to simulate changes in the anomalous SST and was coupled with an anomalous atmospheric model for ENSO simulation. It has been subsequently modified by Seager et al. (1988) and Chang (1994) to include surface heat flux forcing for simulating changes in the total SST field. The version used here closely follows that of Chang et al. (1996).

When the atmospheric and oceanic components are coupled, the observed annual mean wind stress is added to the anomaly fields produced by the empirical atmosphere to form complete surface wind forcing for the ocean. Before coupling the oceanic component to the atmospheric component, a mean SST field produced by an initial 3-yr spinup of the ocean model forced by observed annual mean surface wind stress and heat flux is removed. Therefore, the model mean state is maintained by the observed annual mean surface forcing. The coupling between the two components is done every 6 days. To produce the seasonal cycle, the model is forced by the monthly mean surface heat flux climatology of A. M. da Silva et al. (1995, personal communication). The flux Q is decomposed into six Fourier components so their values at each time step can be precisely determined, namely, $Q = Q_m + A \sum_{n=1,6} Q_n$, where Q_m is the annual mean heat flux, Q_n is a Fourier component of seasonally varying heat flux, and A is an adjustable coefficient that controls the strength of the seasonal heat flux forcing. To prevent the model from drifting from its climatological mean state in long-term integrations, a heat flux correction of the form $-\gamma(T - T_{\text{mean}})$ was used, where γ is taken to be 1/150 day^{-1} and T_{mean} is the observed annual mean sea surface temperature. The domain spans from eastward 120°E to 80°W in longitude and northward from 30°S to 30°N in latitude with a grid size of 2° × 1°. A leapfrog scheme is used for time integration with a time step of 3 h.

The seasonal cycle of the wind stress is determined internally by the model's SST in the same fashion as the anomalous wind stress. In this sense the presented model may be considered as a departure from ''usual'' anomaly coupled models, such as the Lamont model, where the seasonal cycle is prescribed. The advantage of our approach is that it not only captures the dynamics of interannual variability, but also some aspects of interactions between the seasonal cycle and interannual variability. On the other hand, the observed climatological heat flux is specified so that the seasonal cycle in the model is still tightly constrained compared to that in reality. The treatment of the seasonal cycle may also suffer from other shortcomings. First, the thermodynamic air–sea feedbacks of relevance to the tropical annual cycle, such as those that involve low-level stratus clouds (Philander et al. 1996) and wind-induced evaporation (Xie and Philander 1994), are not included. Second, the mean state of the coupled model is prescribed, rather than being determined internally by model physics. Strictly speaking, the seasonal cycle and mean state are an integral part of the coupled system. The conditions of the mean state can have an impact on both the annual cycle and interannual variability.

Even with this modest attempt to allow certain interactions between the seasonal cycle and interannual oscillations, there is no assurance that the model will capture salient features of both the observed seasonal and ENSO cycle. It remains to be proven that the coupled model with a partially active seasonal cycle is actually capable of simulating both the interannual and seasonal variabilty realistically. For this purpose a 100-yr integration was performed with $\delta = 1.53$. For this particular coupling strength the model exhibits interannual self-sustained oscillations with a period of 3.4 yr (Fig. 1), which is well within the observed time period range from 2 to 5 years between successive warm events.

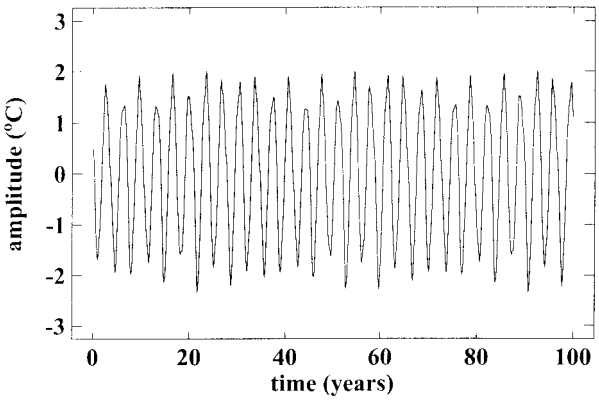

FIG. 1. SST anomalies about the seasonal cycle from a 100-yr integration of the intermediate coupled model with coupling strength $\delta = 1.53$. The time series is averaged over the Niño3 area.

Although we cannot make a direct comparison of the coupled model results with observations, we can ask if the spatial distributions of the simulated standard deviation of the interannual variability and the seasonal cycle are, in a statistical sense, similar to those in reality. Figure 2 displays the spatial patterns of these quantities along with the observed and simulated annual means. Overall, the agreement between observation and simulation is good. There are only minor differences between the annual mean fields, which is expected because of the flux correction toward the observed annual mean SST (Figs. 2a, b). The observed spatial pattern of the annual cycle is also simulated quite well (Figs. 2c, d). Both patterns show a tongue of maximum SST variability with 2°C amplitude located in the far eastern equatorial Pacific slightly south of the equator. Finally, the corresponding patterns for the interannual variability have the characterictic ENSO tongue in common, which extends far to the west and is nearly symmetric about the equator (Figs. 2e, f).

3. Prediction experiments for the standard case

Our analysis in the previous section showed that, at least in a statistical sense, the coupled model is capable of simulating both the annual cycle and the ENSO-related SST variability simultaneously. In this and the following section, we shall perform a more strict test by carrying out prediction experiments in the presence of a partially active seasonal cycle. Our intention is not to improve the forecast skills of existing anomaly mod-

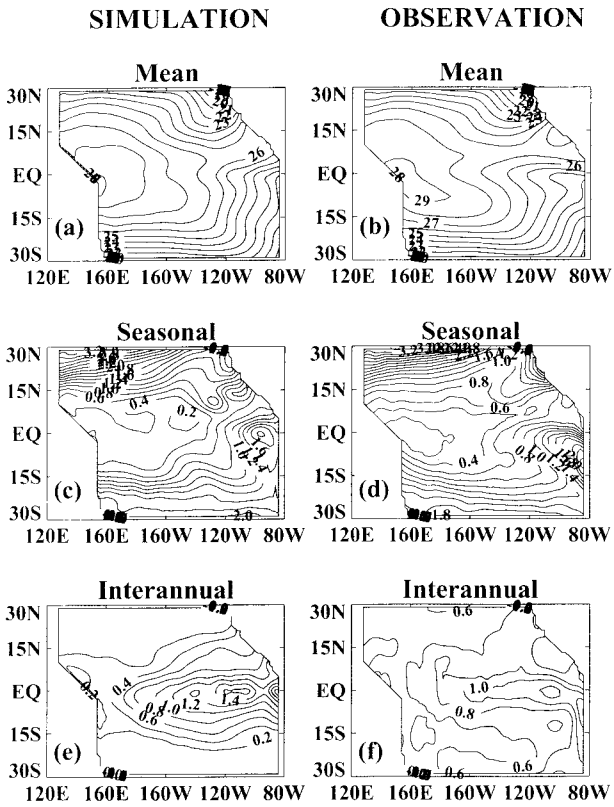

FIG. 2. Spatial SST distribution of (a) the simulated annual mean, (b) the observed annual mean, (c) the standard deviation of the simulated seasonal cycle, (d) the standard deviation of the observed seasonal cycle, (e) the standard deviation of the simulated interannual variability, and (f) the standard deviation of the observed interannual variability.

els by including more realistic physics into the coupled system, but instead to gain insight into the role of the seasonal cycle on ENSO predictions. We, therefore, systematically investigate the predictability of ENSO-related SST anomalies and SST annual cycle with different seasonal backgrounds. Predicting the SST annual cycle would, of course, be trivial in an anomaly model, but since the SST climatology is not prescribed in the present coupled model, it is by no means assured that the seasonal cycle will retain its correct phase and amplitude at long lead times. For these reasons, we have conducted large ensembles of prediction experiments to estimate skills of our coupled model. In order to make the description of the experiments unambiguous we define the following quantities.

SSTM ≡ annual mean of the sea surface temperature over 1950–89. SSTM can be from observation ($SSTM^o$), hindcast uncoupled ocean run ($SSTM^h$), or from model forecast ($SSTM^f$).

SSTS ≡ seasonal cycle with SSTM removed. Renditions of SSTS include $SSTS^o$, $SSTS^h$, and $SSTS^f$.

SSTA ≡ SST anomaly about the seasonal cycle, that is, SSTA = SST − (SSTS + SSTM). Renditions of SSTA include $SSTA^o$, $SSTA^h$, and $SSTA^f$.

a. Standard prediction experiment

In all the experiments shown below, the model was spun up for 3 yr to reach an equilibrium state, starting with $SSTM^o$ as the initial condition. From the fourth year of the model integration the ocean is forced with the observed surface windstress over 40 yr from January 1950 to December 1989 as given by the COADS dataset (A. M. da Silva et al. 1995, personal communication). Additionally, in the first set of experiments the observed net seasonal surface heat flux is used. The initial conditions for the prediction experiments were taken from this hindcast experiment. Predictions were initialized every month and had a duration of 2 yr. During the prediction integration, the evolution of the SST and winds, as well as other variables, is solely determined by the coupled model without adding any further information. We considered the prediction results initialized from January 1951 to December 1989. The total number of analyzed predictions is 468.

We analyzed instantaneous values of SSTs evaluated at the end of each calendar month. Using instantaneous values rather than monthly means can be justified because of the long persistence of SST anomalies. Analyses were performed for both the Niño3 SST (an index defined by spatially averaging SST over 5°N–5°S, 150°–90°W in the eastern equatorial Pacific and Niño4 SST (an index defined by spatially averaging SST over 5°N–5°S, 160°E–150°W in the western equatorial Pacific (Fig. 3a). The ocean model's performance in the hindcast experiment is shown in Figs. 3b and 3c. The correlation between the observed Niño3 time series ($SSTA^o$) and simulation ($SSTA^h$) is 0.53. It is evident from Fig. 3b that the low-frequency variability is well simulated. The modest correlation value 0.53 may be due to the fact that 1) the high-frequency variability in the observations is not captured by the model (the correlation increases to 0.57 when the time series were smoothed with a 5-month running mean), and 2) the low correlation level during the 1950s and 1960s contaminates the overall correlation, which is partially due to the poor quality in the forcing fields. Indeed, the correlation between the two time series increases to 0.68 when only the 1970s and 1980s are considered, which is comparable to other ENSO prediction models (e.g., Goswami and Shukla 1991; Latif and Flügel 1991). Surprisingly, the correlation between the observed and simulated Niño4 time series has a high value of 0.70 (Fig. 3c). This result encourages us not only to investigate model skills in the eastern tropical Pacific, but also in the western part as well.

The results of the prediction experiments are compared to those of the persistence forecasts, which assume

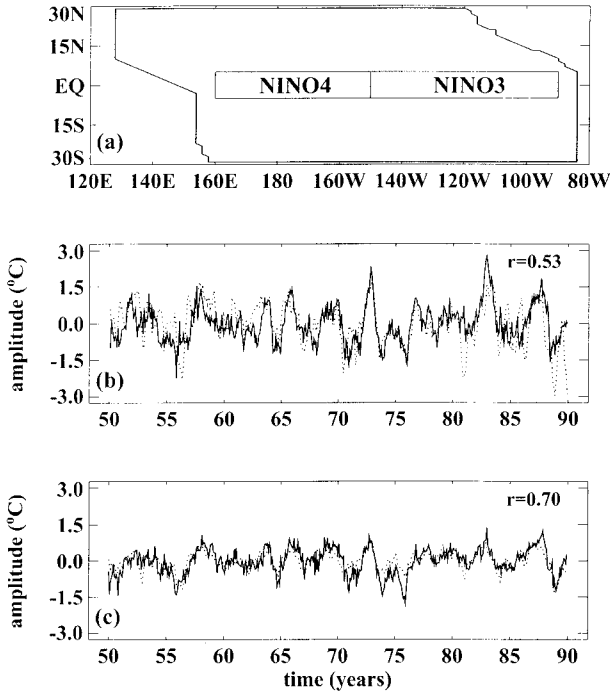

FIG. 3. (a) Niño3 and Niño4 areas. Comparison between the observed SST time series ($SSTA^o$) and simulation ($SSTA^h$) averaged over (b) the Niño3 area and (c) the Niño4 area.

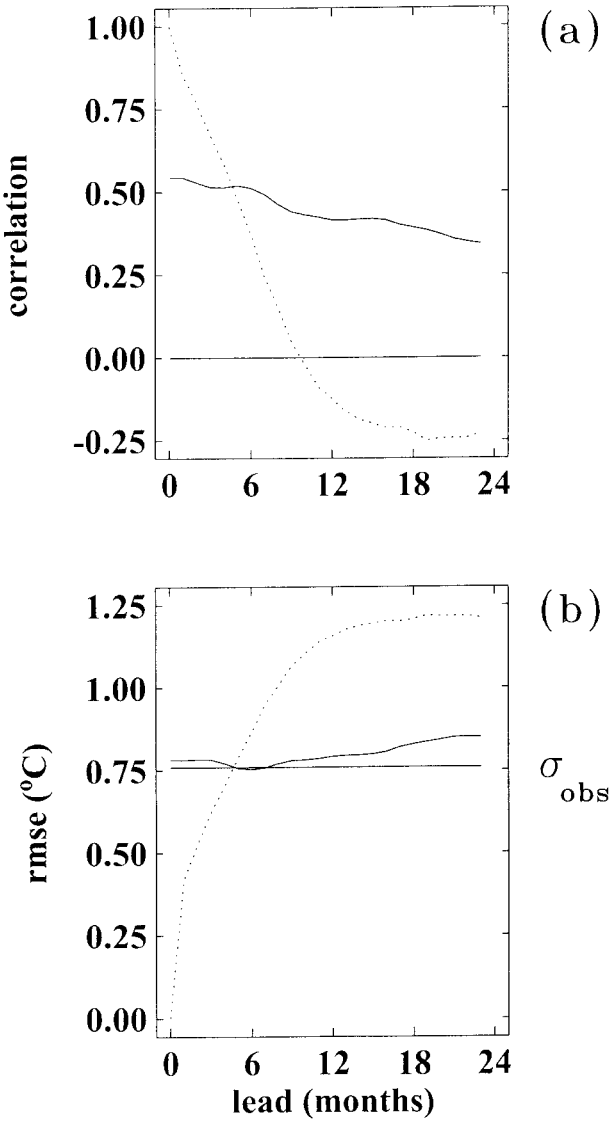

FIG. 4. Prediction skills of the coupled ocean–atmosphere model in Niño3 region: (a) Correlation r($SSTA^o$, $SSTA^f$) and (b) rms error. Dotted line: persistence; solid line: coupled model.

the persistence of the initial ocean state. As in other studies, we use the correlation skill and the root-mean-square (rms) error to measure the phase and amplitude error, respectively. The ocean model's skill is evaluated by comparing the observed interannual variability ($SSTA^o$) to the forecasts, that is, $SSTA^f = SST^f - (SSTS^f + SSTM^f)$, where SST^f is the forecasted total SST. As expected, the persistence forecasts for the Niño3 $SSTA^o$ yields good correlation skill with values above 0.5 for lead times up to nearly 5 months (Fig. 4a). The correlation derived from the coupled model is, therefore, inferior to the persistence forecast for very short lead times. However, at longer lead times the coupled ocean–atmosphere model is clearly superior to the persistence forecast. At lead times of 6–18 months the model predictions still yield significant correlations, while the correlations derived from the persistence forecasts are already insignificant. At longer lead times, the persistence becomes negative, as expected from the quasiperiodicity of ENSO, while the model's correlations are about 0.4 up to 18 months. Although caution must be taken in interpreting the result at these skill levels, it is evident from a direct comparison between predicted ($SSTA^f$) and observed ($SSTA^o$) Niño3 time series (Fig. 5a) that the model successfully forecasts at long lead times (e.g., at 18 months) both the amplitude and phase of the 1957/58, 1982/83, and 1986/87 El Niños as well as the 1988 La Niña. The persistence forecast, on the other hand, predicts these major events far too late (Fig. 5b). The situation is less obvious around the 1972/73 El Niño and the following weak warm event in 1976. Overall, the model's prediction skill is relatively poor during the 1970s. This feature, however, is not unique to the presented coupled model. Other anomaly models have shown similar problems (e.g., Chen et al. 1995; Balmaseda et al. 1995). Possible reasons for the poor skill of the coupled model during this period will be discussed further below.

The evolutions of the rms error (Fig. 4b) show rapid initial error growth for the persistence forcasts, while the initial error of the model forecasts is already at the level of the observed standard deviation σ_{obs}. At about 6 months lead time the rms error of the persistence forecasts exceeds both σ_{obs} and the rms error of the

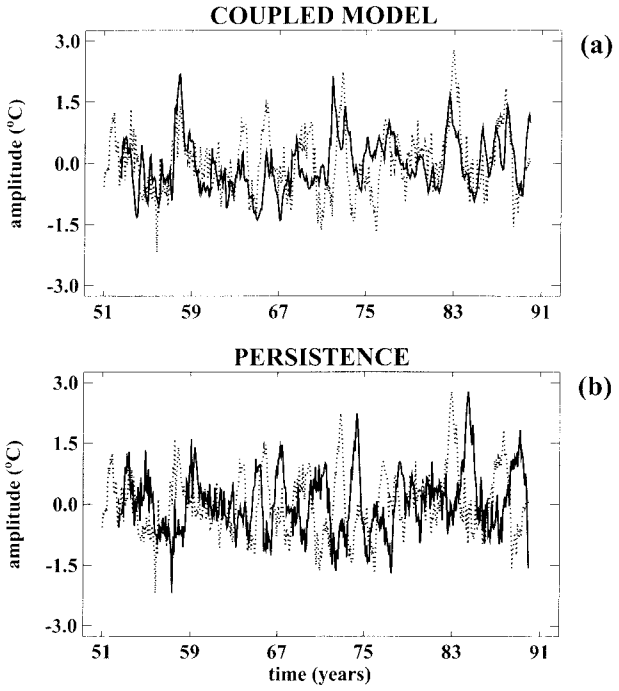

FIG. 5. The 18-month lead time forecast of Niño3 time series ($SSTA^f$) (solid line) of (a) the coupled model and (b) persistence. Dotted line: observation.

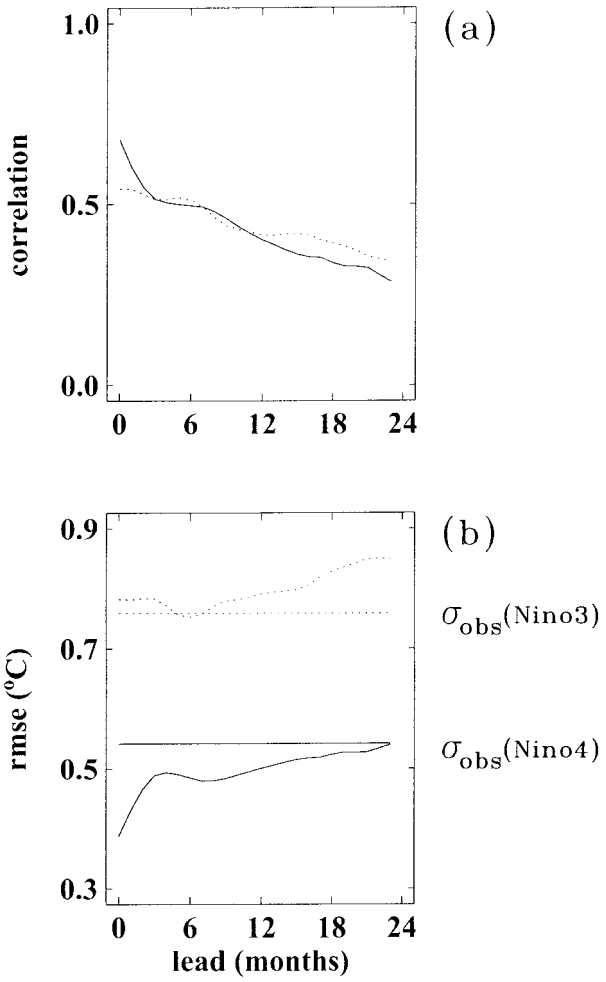

FIG. 6. Model's forecast skill in Nino4 area (solid lines): (a) Correlation and (b) rms error. Dotted lines show the forecast skills of Nino3 SST.

model forecasts. The latter stays nearly constant up to 2 years lead time.

As mentioned earlier, the initial SST conditions in the Niño4 area are more accurate than those in the Niño3 region, but the coupled model yields slightly worse forecasts in the former than in the latter with respect to the phase (Fig. 6a). While in the eastern equatorial Pacific the correlation stays at a level of 0.4 up to lead times of 18 months, the skill drops to about 0.3 in the west. The initial rms error for the interannual Niño4 SST is much smaller than that of Niño3, but beyond 3 months lead time the amplitude errors in both areas are roughly of the same magnitude compared to their respective observed standard deviation (Fig. 6b). In spite of the relatively low correlation of 0.31 between the interannual observed Niño4 SST ($SSTA^o$) and the 18-month lead time predicted interannual Niño4 SST ($SSTA^f$), a direct comparison of the two time series reveals that the coupled model is capable of capturing all major ENSO events in the western Pacific region with the exception of the 1970s (Fig. 7a). Furthermore, the overall prediction skills are clearly superior to the corresponding persistence (Fig. 7b).

b. Decadal dependence of the predictability

Since the verification period is almost 40 years long, it is interesting to examine the decadal dependence of the model's prediction skills. Several recent studies have pointed to the existence of interdecadal ''shifts'' of the background state of the tropical Pacific Ocean (e.g., Zhang et al. 1996; Graham 1994). It has been speculated that these shifts could change the character of ENSO variability on decadal timescales and thus have an impact on ENSO predictability (Gu and Philander 1997; Latif et al. 1997).

To shed some light on this issue, we computed the correlation skills and the rms errors seperately for each of the four decades, that is, 1950s, 1960s, 1970s, and 1980s. Each decadal subset contains 120 predictions, except for the 1950s subset in which the first year prediction was eliminated so that it consists only of 108 predictions. The size of each decadal ensemble should be large enough to yield statistically reliable results.

The predicted SST anomalies ($SSTA^f$) are compared to the observed anomalies ($SSTA^o$) in each of the four decades and the resulting correlation skills and rms errors are shown in Fig. 8. With respect to the phase, the coupled model gives the best predictions during the 1950s and the 1980s. For both these decades the value

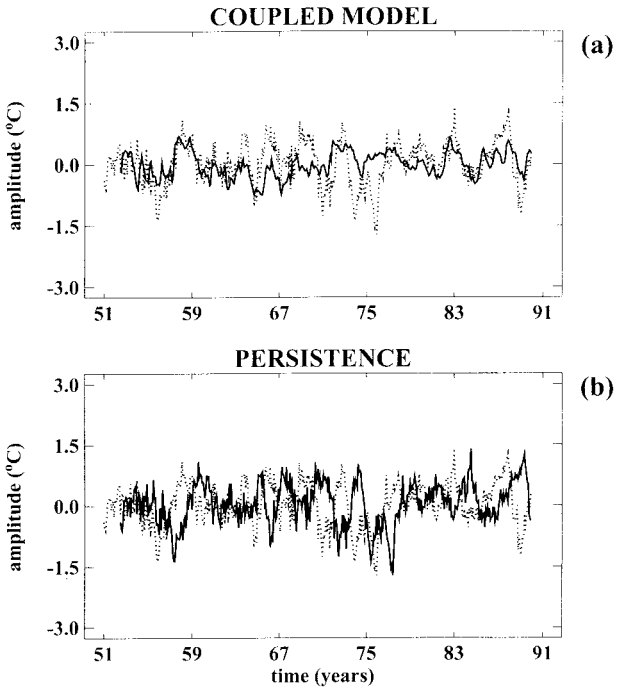

FIG. 7. Same as Fig. 5 except for Nino4 area.

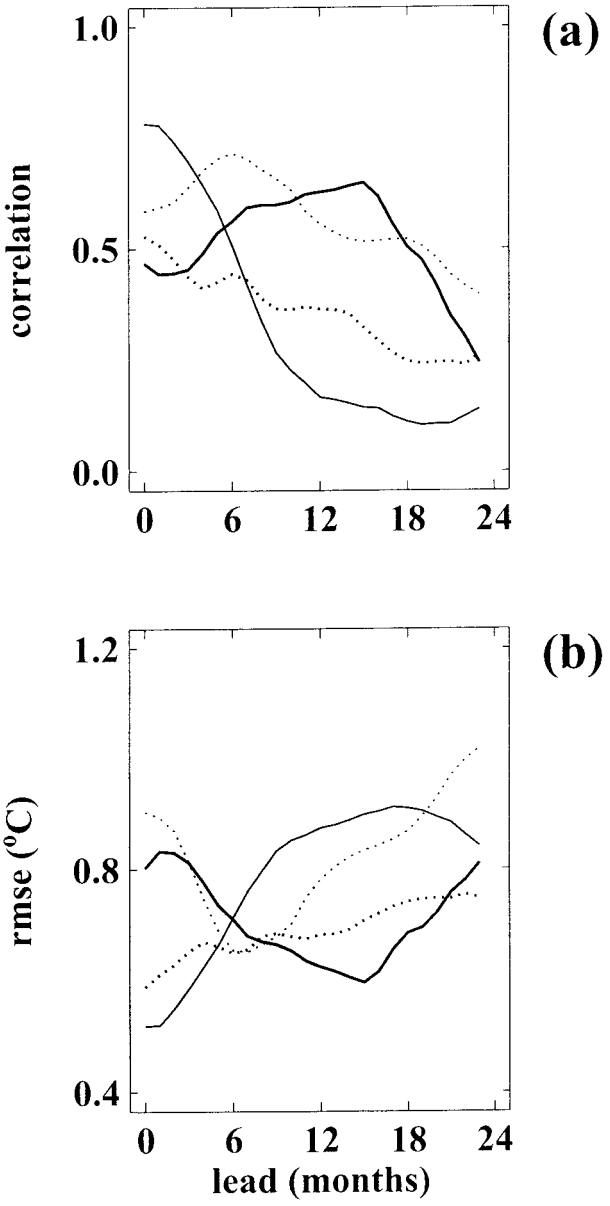

FIG. 8. Decadal dependence of the model forecast skills for Niño3 SST. (a) Correlation r(SSTA^o, SSTA^f) and (b) rms error. Thick solid line: 1950s; thick dotted line: 1960s; thin solid line: 1970s; thin dotted line: 1980s.

of the correlation skills stays higher than 0.5 up to lead times of 1.5 years. The performance of the model forecasts for the other two decades, namely, the 1960s and the 1970s, is relatively poor. While during the 1960s the model forecasts at least beat persistence and yielded values around 0.3 for lead times up to 15 months, the model performance in the 1970s can barely keep up with the persistence forecasts, in spite of the fact that the initial conditions in this decade are most accurate with a correlation value of nearly 0.8.

The time development of the corresponding rms errors for the four decades roughly ''mirrors'' the correlation skills; that is, small rms errors correspond to high correlations and vice versa (Fig. 8b). For example, the remarkably small rms errors for the 1950s occurring at 16 months lead time correspond very well to high correlation skills. Similar features can be found in the other decades. The 1970s are again the least predictable in terms of rms errors, in spite of the smallest initial error.

To examine whether the seasonal dependence of the prediction experiments shows any decadal modulations, we further calculated correlation skills as functions of the month of initialization and the lead time for the four decades (Fig. 9). By doing so, the number of entries for each subset is now reduced to only 10 predictions for a given decade. Because of the small ensembles the results must be interpreted with caution. Nevertheless, these results can help to identify major features of the seasonal dependence of the model's correlation skills. A comparison between the four decades reveals a similarity between the 1950s and 1980s (Figs. 9a, d) on the one hand, and some resemblance between the 1960s and 1970s (Figs. 9b, c) on the other hand. The overall performance of the model forecasts are better for the former group than for the latter group. Results show that predictions initialized during the 1960s and 1970s exhibit a more seasonal-dependent skill than those initialized during the 1950s and 1980s. In particular, during the 1970s the correlation skill of our model experiences sharp decreases during the spring. Our findings are consistent with an earlier result in Balmaseda et al. (1995),

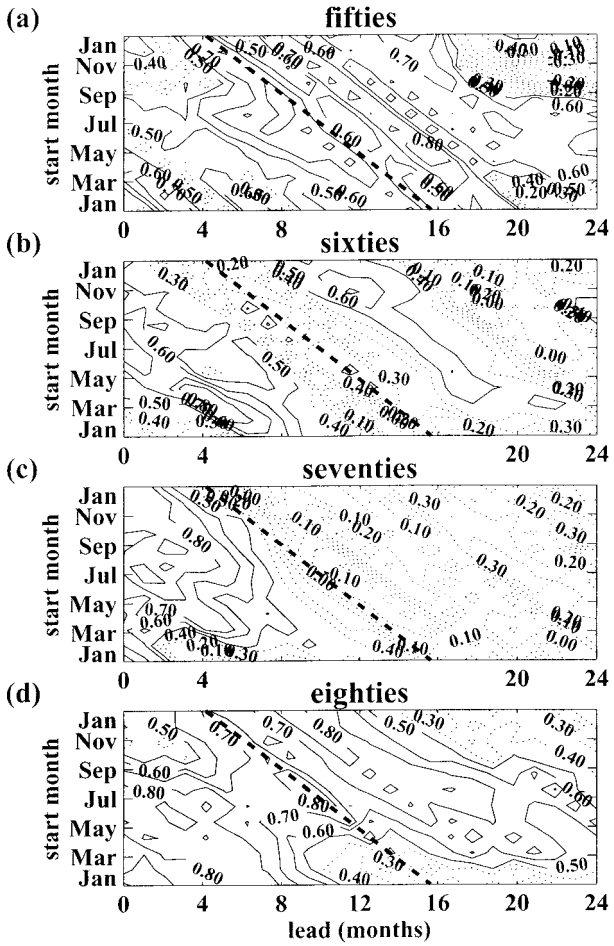

FIG. 9. Seasonal dependence of the model's correlation skill r(SSTA^o, SSTA^f) for the decadal subsets in Niño3 area for the (a) 1950s, (b) 1960s, (c) 1970s, and (d) 1980s. The correlations are shown as functions of the month of initialization and the forecast lag. A heavy dashed line is drawn in each panel to indicate the April crossing for each initialization month.

where a similar analysis was performed only for the 1970s and 1980s.

c. Prediction of the seasonality of SST

As mentioned earlier, because the seasonal cycle is determined by the model itself rather than being prescribed, there is no assurance that the model can retain the correct amplitude and phase of the seasonal cycle at long lead times. To check this, we computed the ''predicted'' seasonal cycle for different lead times from the 468 prediction experiments. For each given month, there are 39 predictions. A comparison between the observed (SSTS^o) and predicted (SSTS^f) Niño3 annual cycle is shown in Fig. 10 at 0-, 6-, 12-, and 18-month lead times. At zero lead time, the amplitude of the seasonal cycle is underestimated and the simulated seasonal cycle lags behind the observation by 1–2 months. At longer lead times, the predicted annual cycle deviation agrees better

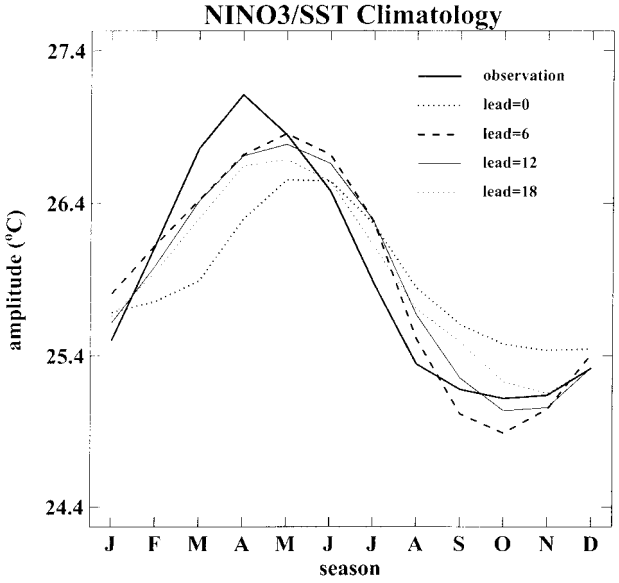

FIG. 10. Predicted Niño3 SST climatologies for lead=0 months (thick dotted line), 6 months (thick dashed line), 12 months (thin solid line), 18 months (thin dotted line), and observations (thick solid line).

with the observation. Overall, the coupled model satisfactorily reproduces the seasonal variation of the equatorial SST. Therefore, we conclude that the presented model posesses respectable prediction skills over the entire tropical Pacific for the 40-yr period and is suitable for further sensitivity studies with modified seasonal backgrounds.

4. Sensitivity experiments

We have shown that the presented coupled model is able not only to predict the interannual variability in the equatorial Pacific, but also to maintain simultanously its own realistic SST annual cycle deviation at longer lead times. In this section, three additional sets of prediction experiments are carried out using the same model, but with modified seasonal forcing. The results will be compared to those of the standard case in order to gain insight into the role of the seasonal cycle on ENSO predictions.

The model initialization runs for the sensitivity experiments were carried out in the same manner as in the standard case, except that seasonal forcings of the surface heat flux and wind stress were artificially modified when the initial conditions were generated. In case a, the seasonal variations of heat flux and wind stress were completely suppressed. In case b, amplitudes of heat flux and wind stress seasonal cycle deviation were increased by a factor of 1.5 while keeping the phase intact. In case c, the phase of the seasonal cycles was shifted by half a year (i.e., January forcing conditions are replaced by July, February conditions by August, and so on), while the amplitudes remain unaltered. For

all four cases the prediction integrations use the same atmospheric feedback (as described in section 2). The seasonal surface heat flux forcing in each prediction experiment remains the same as was specified during the respective initialization run. This procedure assures that the initial conditions are compatible with the coupled prediction integrations.

The model's skill at forecasting ENSO was evaluated for each case by comparing the observed Niño3 SST index ($SSTA^o$) with the predicted Niño3 index ($SSTA^f$). The latter was computed for each case by subtracting from the total predicted temperature (SST^f) both the predicted mean SST ($SSTM^f$) and the forcasted annual cycle deviation ($SSTS^f$), that is, $SSTA^f = SST^f - (SSTS^f + SSTM^f)$. The correlation skills and rms errors from the three experiments are displayed in Fig. 11, along with the standard case. It is clear that both predictive scores drop systematically as the amplitude of the seasonal cycle is increased from 0 to 1.5, although the overall changes are quite small compared to the large modifications made to the seasonal cycle. Still, it is interesting that the ''no seasonal cycle'' case (a) yields the best forecasts. This hints at some model errors since the evolution of total field in these forecasts has to be less like that in nature. One possible reason might be that the treatment of the seasonal cycle in the presented model is, as already mentioned, partially constrained in the sense that the heat flux forcing for the annual cycle is specified rather than allowed to adjust internally. Also, one should bear in mind that the difference in the performance between case a without the seasonal cycle and the standard case with the seasonal cycle is, though systematic, minor (Fig. 11). Since the correlation skills are rather modest these differences might not be too meaningful. Interestingly, in case c where the phase of the seasonal forcing was shifted, the impact on the overall predictive skills is the least significant.

The similarity among model's forecast skills in all three cases with respect to the reference is also reflected in the forecasted Niño3 index ($SSTA^f$). Figures 12 and 13 depict these time series at 12- and 18-month lead time, along with the corresponding power spectra. For comparison, the observed interannual variability (Niño3 $SSTA^o$) was included in each panel. In all cases the modeled power spectra agree very well with the observations at both lead times although the observed spectra are slightly underestimated, presumably because of the absence of high frequency noise in the forcing. Overall there are only subtle differences among the four predicted time series for a given lead time (Figs. 12a–d at 12-month lead and Figs. 13a–d at 18-month lead time). For example, a detailed comparison between case a without the seasonal cycle and case b with an artificially enhanced seasonal cycle reveals that the seasonal cycle does contribute to terminate the warm ENSO events. This becomes particularly clear by comparing the 1957/58 and 1972/73 El Niños between these two cases at 1-yr lead time: both transitions from warm to cold states agree better with the observation in case b than those in case a (Figs. 14a,b). In case a, where the seasonal cycle is entirely absent, the model tends to prolong the warming in the eastern equatorial Pacific, while in case c, where the amplitude of the seasonal cycle deviation was enhanced by a factor of 1.5, the termination of the warm events tends to come a few months earlier. This influence of the seasonal cycle on ENSO predictions is, however, not always beneficial, as can be seen in an analogous comparison for the 1982/83 warm event (Fig.

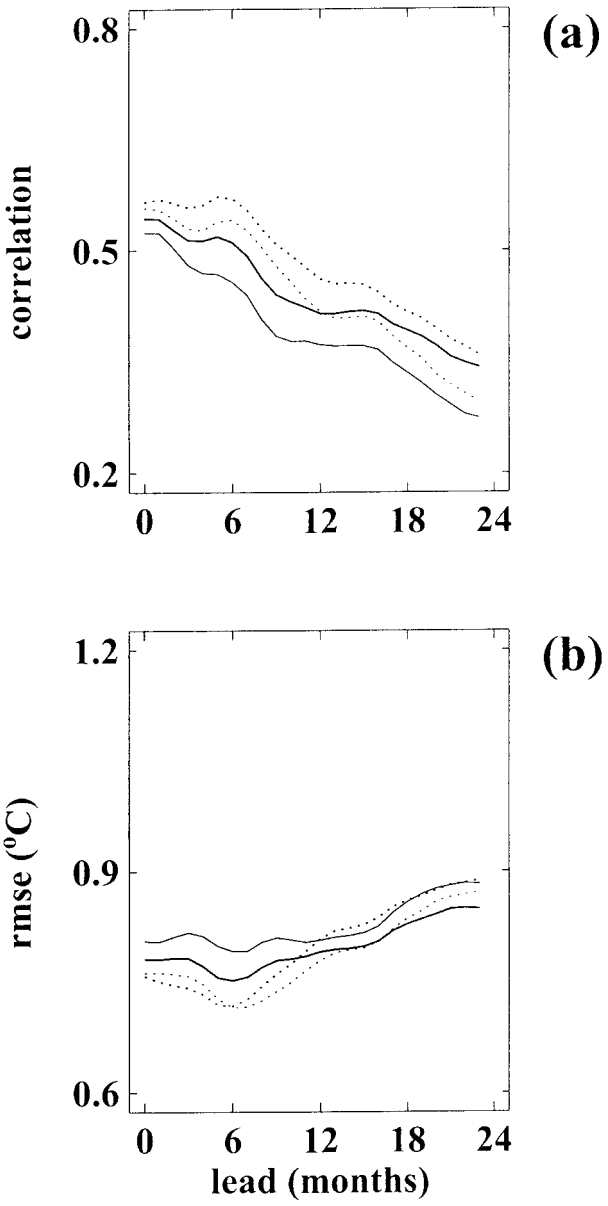

FIG. 11. Model's forecast skills in Niño3 region with different seasonal background. (a) Correlations r($SSTA^o$, $SSTA^f$) and (b) rms errors. Thick solid line: reference case; thick dotted line: case a; thin solid line: case b; thin dotted line: case c.

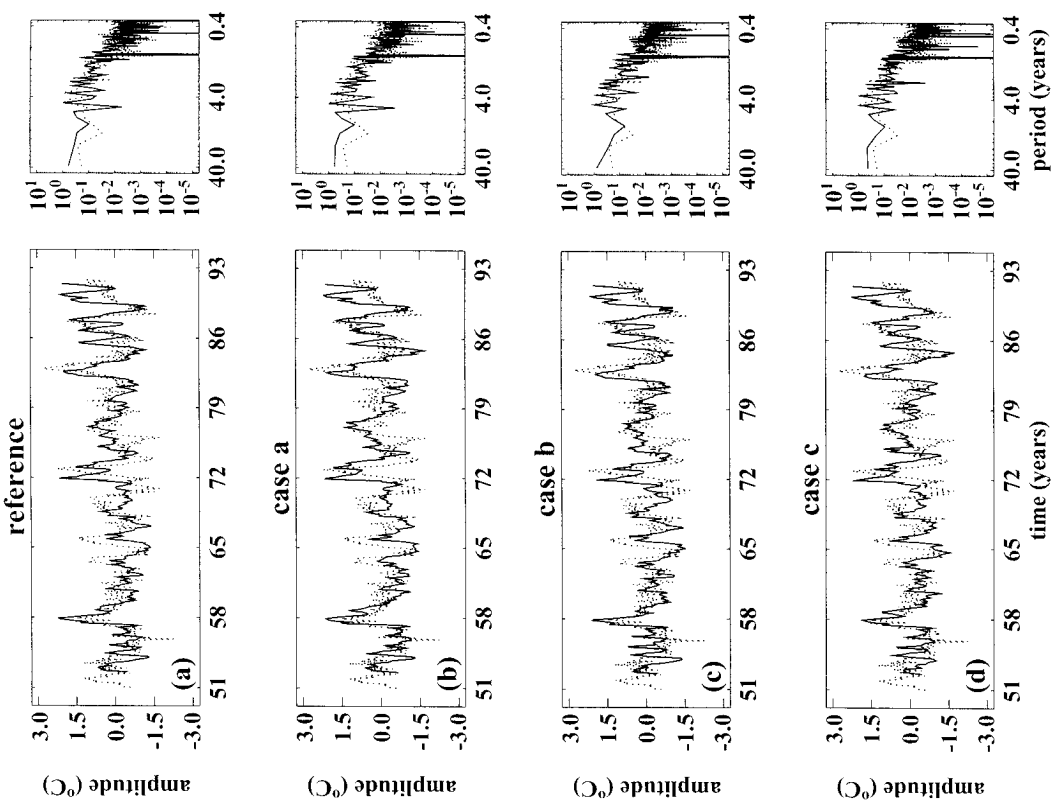

FIG. 12. The 12-month lead time forecast of Niño3 time series (SSTA') and power spectra for (a) reference case, (b) case a, (c) case b, and (d) case c.

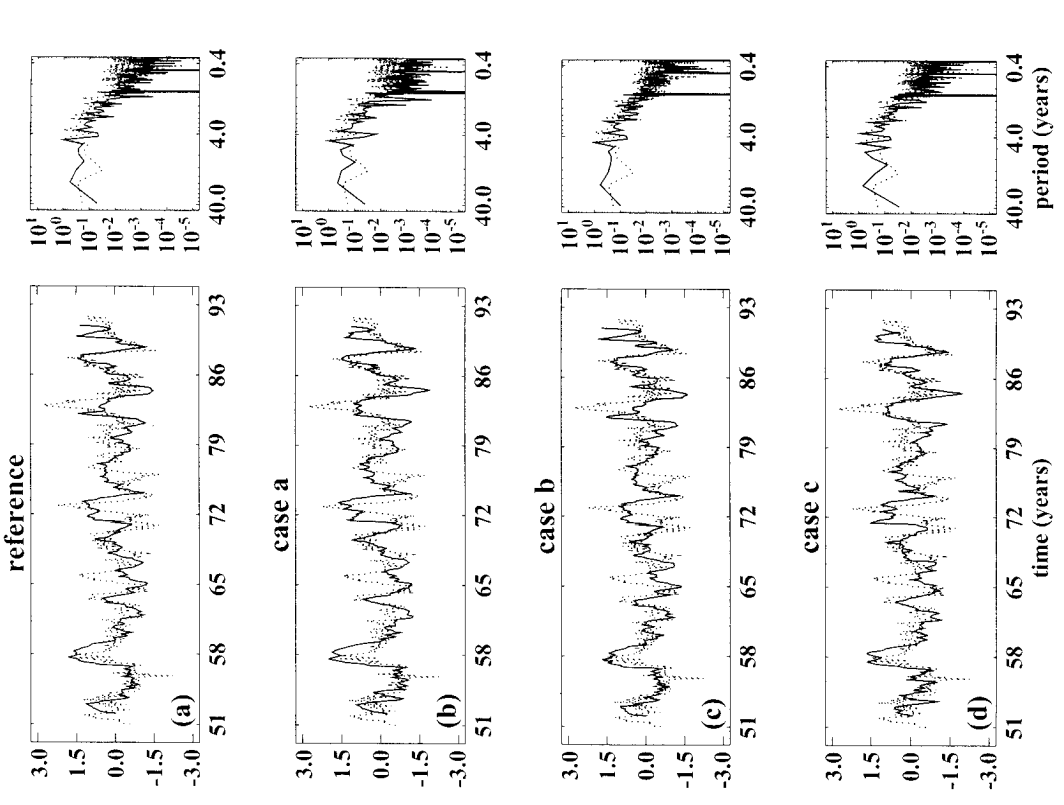

FIG. 13. Same as Fig. 12, but for 18-month lead time.

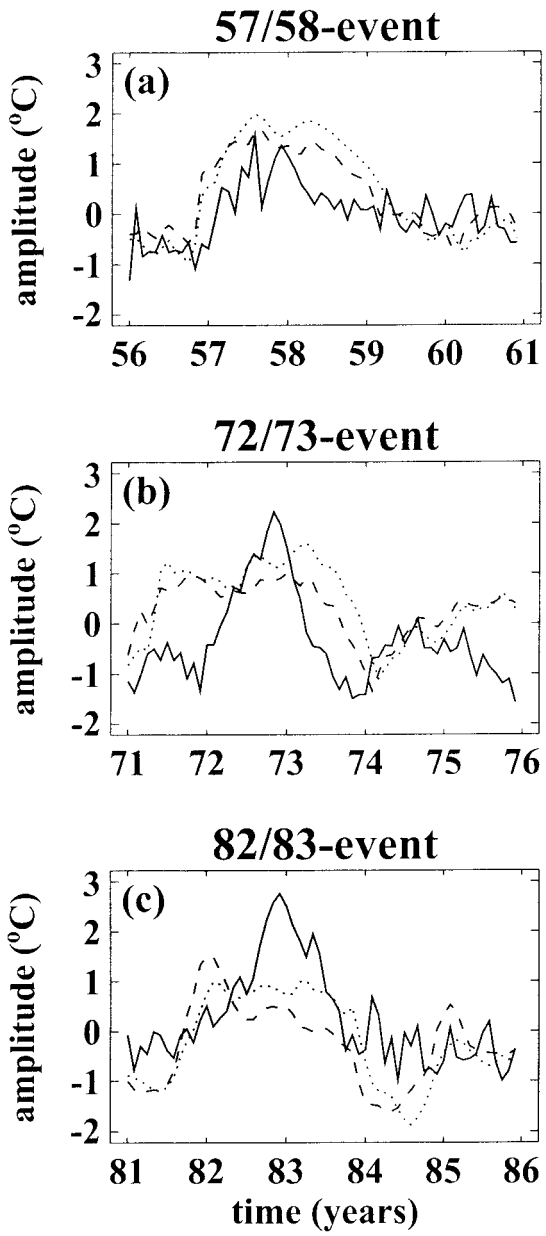

FIG. 14. The 12-month lead time forecast of Niño3 SST for (a) the 1957/58 El Niño, (b) the 1972/73 El Niño, and (c) the 1982/83 El Niño. Solid line: observation; dotted line: case a; dashed line: case c.

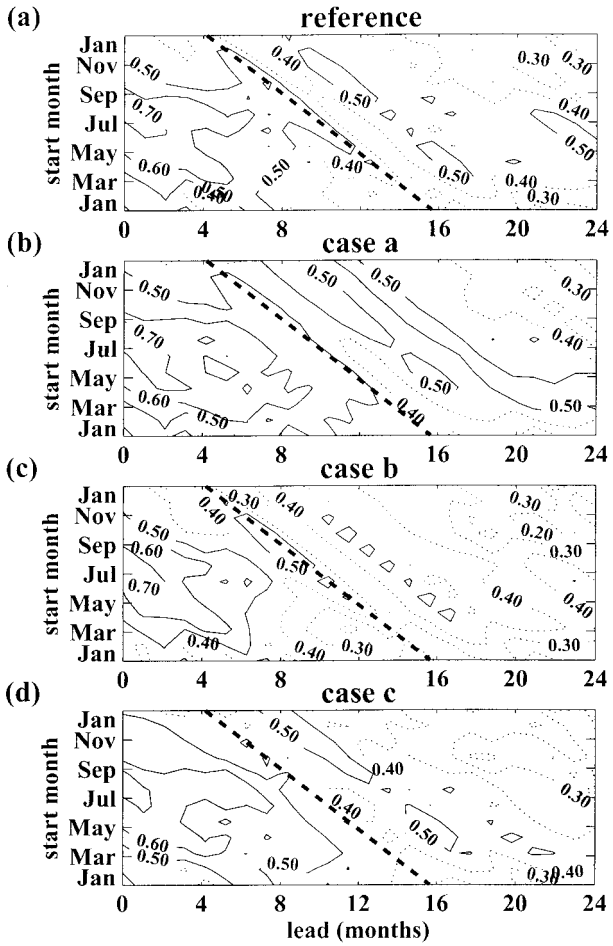

FIG. 15. Seasonal dependence of the model's correlation skills $r(SSTA^o, SSTA^f)$ in Niño3 area for (a) the reference, (b) case a, (c) case b, and (d) case c. The correlations are shown as functions of the month of initialization and the forecast lag. A heavy dashed line is drawn in each panel to indicate the April crossing for each initialization month.

14c), where clearly case a in the absence of a seasonal cycle yields better results.

In order to investigate the seasonal dependence of the predictability, we computed the correlation skills in all four cases as a function of the starting month and the lead time (Fig. 15). By doing so, the number of entries for each subset is reduced to 39, so that the results are still statistically reliable. An especially noticable feature in all four cases is the spring predictability barrier, a phenomenon that has been noted in other ENSO prediction models (Latif and Flügel 1991; Balmaseda et al. 1995; Chen et al. 1995; Chen et al. 1997). During the spring, the correlation skills experience sharp decreases. The fact that the spring barrier occurs even in the absence of a seasonally varying background (Fig. 15b) or in the presence of an artificially phase-shifted seasonal cycle (Fig. 15d) raises the possibility that the seasonal dependence of the skill is largely determined by the seasonal information already hidden in the initial conditions of the predictions. Another possibility that will be further discussed in the next section is that the presented model underestimates the nonlinear interaction between the seasonal cycle and the interannual variability.

The impact of the seasonal cycle on ENSO predictability varies only slightly from decade to decade: the correlation skills derived from the decadal subsets (see section 3b) differ by a small margin among each other for each of the four decades with the least significant

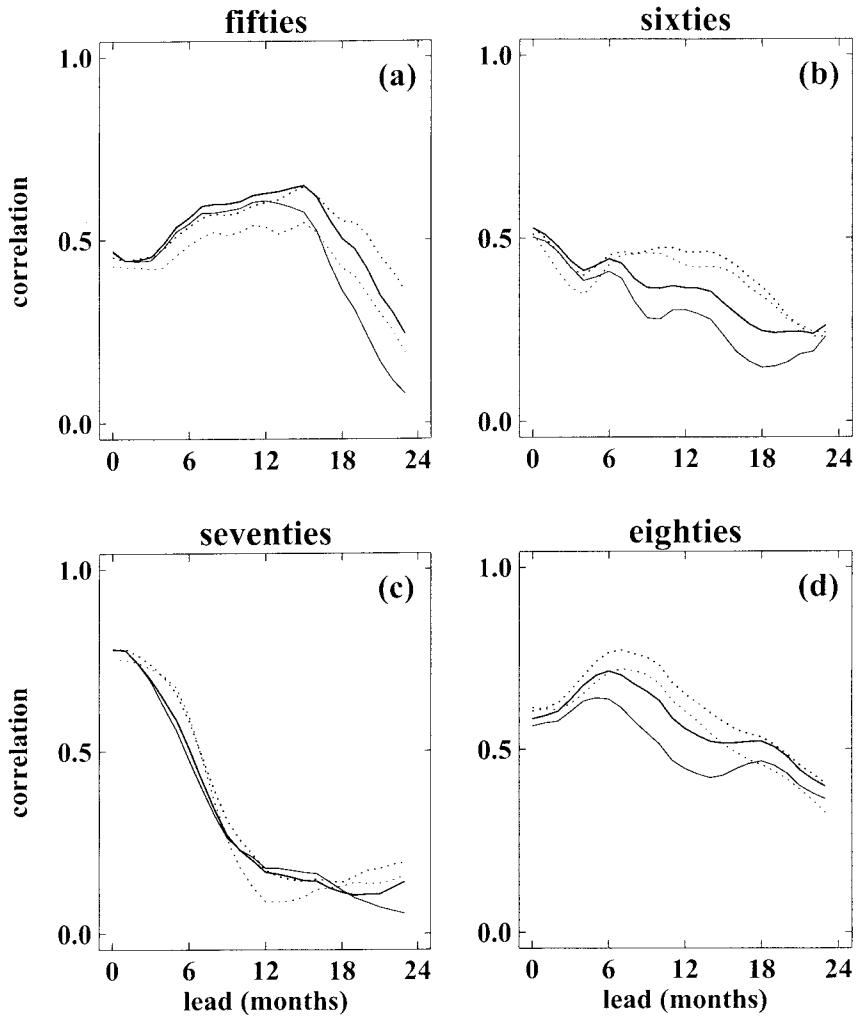

FIG. 16. Decadal dependence of the model's correlation skills in Niño3 region for different seasonal backgrounds. (a) The 1950s, (b) 1960s, (c) 1970s, and (d) 1980s. Thick solid line: reference; thick dotted line: case a; thin solid line: case b; thin dotted line: case c.

changes during the 1970s (Fig. 16). As in the skills based on the total ensembles (Fig. 11), the prediction skills in the decadal subsets decrease in general slightly as the amplitude of the seasonal cycle increases. Furthermore, a phase shift in the seasonal forcing shows little impact on the skills during the 1970s and 1980s (Figs. 16c,d). Interestingly, the predictive skill in this case drops during the 1950s (Fig. 16a), while it improves during the 1960s (Fig. 16b).

5. Summary and discussion

We have investigated the impact of the annual cycle on ENSO predictability in the tropical Pacific using an intermediate coupled ocean–atmosphere model that allows certain feedbacks between the seasonal cycle and interannual oscillations. By conducting large ensembles of prediction experiments, we first demonstrate that this model has respectable forecast skills. We then perform three additional experiments with different phase and amplitude in the seasonal background to gain an understanding of the role of the seasonal cycle in ENSO prediction. Major conclusions of this study can be summarized as follows.

1) Overall, the model's ENSO forecast skills do not show a strong sensitivity to variations in phase and amplitude in the seasonal background.
2) The spring predictability barrier appears as a prominent feature in the model's forecast skills even in the absence of a seasonally varying background.
3) There is a weak dependence of the predictive skills on changes in the amplitude of the seasonal cycle in the sense that the skills decrease systematically by a small margin as the seasonal cycle strengthens.
4) Changes in the phase of the seasonal cycle have little influence on the overall prediction skills.

5) Seasonal dependence of prediction skill is stronger in the 1960s and 1970s and weaker during the 1950s and 1980s.
6) The model gives the best ENSO forecasts at lead times around 18 months in the 1950s and 1980s, while the performance is worst during the 1970s.

The insensitivity of the prediction skills to variations in the seasonal background implies a weak nonlinear interaction between the seasonal cycle and interannual oscillations in the presented model configuration. In fact, to a certain extent, the simulated total SSTs in all the experiments can almost be regarded as a linear superposition of the responses to seasonal and interannual components of the wind forcing. It is possible to increase the nonlinearity of the interaction in the model by increasing the coupling strength. We have repeated the experiments with different coupling strengths and found that when the coupling strengths for both the seasonal and interannual components are higher than 1.8, the sensitivity of the skills to changes in the seasonal cycle become more prominent (not shown). However, we have also found that using such a large coupling strength yields worse prediction skills than those in the standard case, suggesting that the model may reside in an unrealistic parameter regime where the coupling strengths are too large. This result is consistent with earlier studies (Penland and Sardeshmukh 1995; Chang et al. 1996; Eckert and Latif 1997; Flügel and Chang 1996), which suggest that ENSO may be best viewed as a stochastically driven stable process rather than a nonlinearly driven irregular self-sustained oscillator. Having stated the above, one should be reminded that these conclusions only hold within the limitations of the model and do not necessarily reflect the real system.

In regard to the so-called spring predictability barrier, our study confirms previous ones that the predictability is generally worst during the spring (Latif and Flügel 1991; Balmaseda et al. 1995; Chen et al. 1995). The large ensemble used in our study ensures that this is a robust feature of the model. It is interesting that our model with a partially active seasonal cycle exhibits basically the same seasonal dependence of the predictive skill as the anomaly models. Perhaps the most surprising result of this study is that even in the absence of the seasonal cycle, the spring predictability barrier remains, suggesting that the spring predictability barrier may result from seasonal noise structures in the initial conditions rather than from a seasonally varying background. This hypothesis is supported by Y. Q. Chen and D. S. Battisti (1997, personal communication) in similar experiments using their version of the Lamont model. Furthermore, our findings are also consistent with previous reports (Chen et al. 1995; Penland and Sardeshmukh 1995; Penland 1996) that the initial conditions are of prime importance to the seasonal dependence of the predictive skills. These results, however, do not completely rule out the possibility that the seasonally varying background can have an impact on ENSO predictability due to imperfect representation of seasonal cycle and ENSO dynamics by the model.

Consistent with Balmaseda et al. (1995), we found that the severity of the spring barrier undergoes decadal variations with stronger barriers during the 1960s and 1970s and weaker barriers in the 1950s and 1980s.

We end our discussion with a notion on decadal modulation of the ENSO predictability. Although recent studies have given rise to much controversy about the underlying mechanism of the dominant mode on decadal timescales in the Pacific (Latif and Barnett 1994; Gu and Philander 1997; Jacobs et al. 1994; Zhang et al. 1997; Lau and Nath 1996), it is certain that the extension of the decadal patterns reaches far into the extratropics. It has been speculated that the decadal variations may have implications for ENSO in so far as the tropical mean state of the Pacific might undergo variations on decadal timescales. One possible mechanism that causes changes in the mean state of the tropical Pacific is through the remote influence of the extratropical oceans (Deser et al. 1996; Gu and Philander 1997). Recently, Lysne et al. (1997) used data assimilation experiments to demonstrate that during the 1970s a decadal transition from a colder mean state to a warmer mean state initiated in the higher latitudes could propagate into the Tropics, thereby causing shifts in the tropical mean thermocline. As a result of the decadal shift, the characteristics of ENSO during the 1970s may be different from those in the other decades. Interestingly, this period coincides with the decade in which the model's prediction skills are worst. One possible explanation for the poor performance may be that since the model is confined to the Tropics and has a fixed mean depth of the thermocline, it excludes decadal variation of the thermocline caused by remote influences of the extratropical regions. As already pointed out, the poor performance of the prediction experiments during the 1970s is not a unique feature of our model; other regional models also suffer from a similar problem (e.g., Latif and Flügel 1991; Chen et al. 1995; Balmaseda et al. 1995). Whether the different predictive skills in various decades are actually caused by decadal variations in the tropical mean state can only be determined by carrying out forecast experiments with a model that explicitly introduces these decadal fluctuations into the background. Such an investigation is currently under way.

Acknowledgments. We would like to thank D. Battisti and one anonymous reviewer for their helpful and stimulating comments. This research is supported by the Climate and Global Change Program of NOAA under Grant NA46GP0166 and NSF under Grant ATM9616582. P. Chang is also supported by the NSF Young Investigator Award OCE-9357860.

REFERENCES

Balmaseda, M. A., M. K. Davey, and D. L. T. Anderson, 1995: Decadal and seasonal dependence of ENSO prediction skill. *J. Climate,* **8,** 2705–2715.

Barnett, T. P., 1984: Prediction of the El Niño 1982–83. *Mon. Wea. Rev.,* **112,** 1403–1407.

——, N. Graham, M. A. Cane, S. Zebiak, S. Dolan, J. O'Brien, and D. Legler, 1988: On the prediction of the El Niño 1986–1987. *Science,* **241,** 192–196.

——, M. Latif, N. Graham, M. Flügel, S. Pazan, and W. White, 1993: ENSO and ENSO-related predictability. Part I: prediction of equatorial Pacific sea surface temperature with a hybrid coupled ocean–atmosphere model. *J. Climate,* **6,** 1545–1566.

Cane, M. A., S. E. Zebiak, and S. C. Dolan, 1986: Experimental forecasts of El Niño. *Nature,* **321,** 827–832.

Chang, P., 1994: A study of the seasonal cycle of sea surface temperature in the tropical Pacific Ocean using reduced gravity models. *J. Geophys. Res.,* **99,** 7725–7741.

——, and S. G. Philander, 1994: A coupled ocean–atmosphere instability of relevance to the seasonal cycle. *J. Atmos. Sci.,* **51,** 3627–3648.

——, L. Ji, B. Wang, and T. Li, 1995: Interactions between the seasonal cycle and El Niño–Southern Oscillation in an intermediate coupled ocean–atmosphere model. *J. Atmos. Sci.,* **52,** 2353–2372.

——, ——, H. Li, and M. Flügel, 1996: Chaotic dynamics versus stochastic processes in El Niño–Southern Oscillation in coupled ocean–atmosphere models. *Physica D,* **98,** 301–320.

Chen, D., S. E. Zebiak, A. J. Busalacchi, and M. A. Cane, 1995: An improved procedure for El Niño forecasting: Implications for predictability. *Science,* **269,** 1699–1702.

Chen, Y. Q., D. S. Battisti, T. N. Palmer, J. Barsugli, and E. S. Sarachik, 1997: A study of the predictability of tropical Pacific SST in a coupled atmosphere–ocean model using singular vector analysis: The role of the annual cycle and the ENSO cycle. *Mon. Wea. Rev.,* **125,** 831–845.

Deser, C., M. A. Alexander, and M. S. Timlin, 1996: Upper ocean thermal variations in the North Pacific during 1970–1991. *J. Climate,* **9,** 1840–1855.

Eckert, C., and M. Latif, 1997: Predictability of a stochastically forced hybrid coupled model of El Niño. *J. Climate,* **10,** 1488–1504.

Flügel, M., and P. Chang, 1996: Impact of dynamical and stochastic processes on the predictability of ENSO. *Geophys. Res. Lett.,* **23** (16), 2089–2092.

Goswami, B. N., and J. Shukla, 1991: Predictability of a coupled ocean–atmosphere model. *J. Climate,* **4,** 3–22.

Graham, N. E., 1994: Decadal-scale climate variability in the tropical and North Pacific during the 1970s and 1980s: Observations and model results. *Climate Dyn.,* **10,** 135–162.

——, J. Michaelsen, and T. P. Barnett, 1987: An investigation of the El Niño–Southern Oscillation cycle with statistical models. 2, Model results. *J. Geophys. Res.,* **92** (C13), 14 271–14 289.

Gu, D., and S. G. H. Philander, 1995: Secular changes of annual and interannual variability in the Tropics during the past century, *J. Climate,* **8,** 864–876.

——, and ——, 1997: Interdecadal climate fluctuations that depend on exchanges between the tropics and extratropics. *Science,* **275,** 805–807.

Jacobs, G. A., H. E. Hurlburt, J. C. Kindle, E. J. Metzger, J. L. Mitchell, W. J. Teague, and A. J. Wallcraft, 1994: Decade-scale trans-Pacific propagation and warming effects of an El Niño anomaly. *Nature,* **370,** 360–363.

Jin, F.-F., D. Neelin, and M. Ghil, 1994: El Niño on the devil's staircase: Annual subharmonic steps to chaos. *Science,* **246,** 70–72.

——, ——, and ——, 1996: El Niño/Southern Oscillation and the annual cycle: Subharmonic frequency-locking and aperiodicity. *Physica D,* **98,** 442–465.

Latif, M., and M. Flügel, 1991: An investigation of short-range climate predictability of the El Niño/Southern Oscillation in the tropical Pacific. *J. Geophys. Res.,* **96,** 2661–2673.

——, and T. P. Barnett, 1994: Causes of decadal climate variability over the North Pacific and North America. *Science,* **266,** 634–637.

——, A. Sterl, E. Maier-Reimer, and M. M. Junge, 1993: Climate variability in a coupled GCM. Part I: The tropical Pacific. *J. Climate,* **6,** 5–21.

——, R. Kleeman, and C. Eckert, 1997: Greenhouse warming, decadal variability, or El Niño? An attempt to understand the anomalous 1990s. *J. Climate,* **10,** 2221–2239.

Lau, N.-C., and M. J. Nath, 1996: The role of the ''atmospheric bridge'' in linking tropical Pacific ENSO events to extratropical SST anomalies. *J. Climate,* **9,** 2036–2057.

Leetmaa, A., and M. Ji, 1989: Operational hindcasting of the tropical Pacific. *Dyn. Atmos. Oceans,* **13,** 465–490.

Lysne, J., P. Chang, and B. Giese; 1997: Impact of the extratropical Pacific on equatorial variability. *Geophys. Res. Lett.,* **24,** 2589–2592.

Mechoso, C. R., A. W. Robertson, N. Barth, M. K. Davey, P. Delecluse, P. R. Gent, S. Ineson, B. Kirtman, M. Latif, H. Le Treut, T. Nagai, J. D. Neelin, S. G. H. Philander, J. Polcher, P. S. Schopf, T. Stockdale, M. J. Suarez, L. Terray, O. Thual, and J. J. Tribbia, 1995: The seasonal cycle over the tropical Pacific in coupled atmosphere–ocean general-circulation models. *Mon. Wea. Rev.,* **123,** 2825–2838.

Mitchell, T. P., and J. M. Wallace, 1992: On the annual cycle in equatorial convection and sea surface temperature. *J. Climate* **5,** 1140–1156.

Penland, C., 1996: A stochastic model of IndoPacific sea surface temperature anomalies. *Physica D,* **98,** 534–558.

——, and T. Magorian, 1993: Prediction of Niño 3 sea surface temperatures using linear inverse modeling. *J. Climate,* **6,** 1067–1076.

——, and P. D. Sardeshmukh, 1995a: Error and sensitivity analysis of geophysical eigensystems. *J. Climate,* **8,** 1988–1998.

——, and ——, 1995b: The optimal growth of tropical sea surface temperature anomalies. *J. Climate,* **8,** 1999–2024.

Philander, S. G. H., D. Gu, D. Halpern, G. Lambert, N.-C. Lau, T. Li, and R. C. Pacanowski, 1996: Why the ITCZ is mostly north of the equator. *J. Climate,* **9,** 2958–2972.

Rasmusson, E. M., and T. H. Carpenter, 1982: Variations in tropical sea surface temperature and surface wind fields associated with the Southern Oscillation/El Niño. *Mon. Wea. Rev.,* **110,** 354–384.

Rosati, A., K. Miyakoda, and R. Gudgel, 1997: The impact of ocean initial conditions on ENSO forecasting with a coupled model. *Mon. Wea. Rev.,* **125,** 754–772.

Seager, R., S. E. Zebiak, and M. A. Cane, 1988: A model of the tropical Pacific sea surface temperature climatology. *J. Geophys. Res.,* **93** (C2), 1265–1280.

Tziperman, E., L. Stone, M. A. Cane, and H. Jarosh, 1994: El Niño chaos: Overlapping of resonances between the seasonal cycle and the Pacific Ocean–atmosphere oscillator. *Science,* **264,** 72–74.

Woodruff, S. D., R. J. Slutz, R. L. Jenne, and P. M. Steurer, 1987: A comprehensive ocean–atmosphere data set. *Bull. Amer. Meteor. Soc.,* **69,** 1239–1250.

Xie, S.-P., and S. G. H. Philander, 1994: A coupled ocean–atmosphere model of relevance to the ITCZ in the eastern Pacific. *Tellus,* **46A,** 340–350.

Xu, J. S., and H. von Storch, 1990: Principal oscillation patterns—Prediction of the state of ENSO. *J. Climate,* **3,** 1316–1329.

Zebiak, S. E., and M. A. Cane, 1987: A model El Niño–Southern Oscillation. *Mon. Wea. Rev.,* **115,** 2262–2278.

Zhang, Y., J. M. Wallace, and D. S. Battisti, 1997: ENSO-like interdecadal variability: 1900–93. *J. Climate,* **10,** 1004–1020.